Fluorine-18-α-Methyltyrosine Positron Emission Tomography for Diagnosis and Staging of Lung Cancer: A Clinicopathologic Study

Kyoichi Kaira,[1] Noboru Oriuchi,[2] Yoshimi Otani,[3] Kimihiro Shimizu,[3] Shigebumi Tanaka,[4] Hisao Imai,[1] Noriko Yanagitani,[1] Noriaki Sunaga,[1] Takeshi Hisada,[1] Tamotsu Ishizuka,[1] Kunio Dobashi,[6] Yoshikatsu Kanai,[7] Hitoshi Endou,[7] Takashi Nakajima,[5] Keigo Endo,[2] and Masatomo Mori[1]

Abstract

Purpose: L-[3-^{18}F]-α-Methyltyrosine ([^{18}F]FMT) is an amino acid tracer for positron emission tomography (PET). We evaluated the diagnostic usefulness of [^{18}F]FMT PET in non–small-cell lung cancer (NSCLC) patients. Tumor uptake of [^{18}F]FMT was compared with that of 2-[^{18}F]-fluoro-2-deoxy-D-glucose ([^{18}F]FDG) and correlated with L-type amino acid transporter 1 (LAT1) expression.

Experimental Design: Fifty NSCLC patients were enrolled in this study, and a pair of PET study with [^{18}F]FMT and [^{18}F]FDG was done. LAT1 expression and Ki-67 labeling index of the resected tumors were analyzed by immunohistochemical staining.

Results: For the primary tumor detection, [^{18}F]FMT PET exhibited a sensitivity of 90% whereas the sensitivity for [^{18}F]FDG PET was 94%. For lymph node staging, the sensitivity and specificity of [^{18}F]FMT PET were 57.8% and 100%, and those of [^{18}F]FDG PET were 65.7% and 91%, respectively. The expression of LAT1 in squamous cell carcinoma and large cell carcinoma was significantly higher than that in adenocarcinoma. [^{18}F]FMT uptake was also higher in squamous cell carcinoma and large cell carcinoma than in adenocarcinoma. Uptake of [^{18}F]FMT in the tumor is closely correlated with LAT1 expression ($\rho = 0.890$).

Conclusion: [^{18}F]FMT PET had no false-positives in the detection of primary tumor and lymph node metastasis and could improve the diagnostic performance in NSCLC. Uptake of [^{18}F]FMT correlated with the expression of LAT1 that showed a significant association with cellular proliferation.

Lung cancer is the leading cause of cancer-related death in many countries. Eighty percent of the lung cancers are non–small-cell lung cancer (NSCLC) and 20% are small-cell lung cancer (1). Exact staging of patients with lung cancer is of crucial importance in determining appropriate therapeutic management. Although computed tomography (CT) has been widely used for the preoperative evaluation, numerous studies have shown that it is limited for the staging because of its low reliability for lymph node staging (2, 3).

The usefulness of 2-[^{18}F]-fluoro-2-deoxy-D-glucose positron emission tomography ([^{18}F]FDG PET) in cancer diagnosis has been investigated in many studies (4–6). Determination of malignant lesions with [^{18}F]FDG PET is based on the glucose metabolism (7, 8). The overexpression of glucose transporter 1 (Glut1) in human cancer has been shown to be closely related to [^{18}F]FDG uptake (9, 10). Many studies have, however, revealed the lack of specificity in [^{18}F]FDG accumulation because [^{18}F]FDG PET shows increased activity in inflammatory processes, sarcoidosis, or physiologic muscle activity (11). Thus, new PET tracers are being evaluated to improve specificity to detect malignancy (12–16).

We have developed L-[3-^{18}F]-α-methyltyrosine ([^{18}F]FMT) as an amino acid tracer for PET imaging and confirmed its potential usefulness in the detection of neoplasms using experimental tumor models (17–19). [^{18}F]FMT, an amino acid analogue, is accumulated in tumor cells solely via an amino acid transport system (17–21). Clinical trials have shown that [^{18}F]FMT PET is useful to differentiate between benign lesions and malignant tumors (22, 23).

Amino acid transporters are essential for the growth and proliferation of normal and transformed cells (24, 25). Among various types of amino acid transports, system L is a Na^+-independent large and neutral amino acid transport agency (24, 26). L-type amino acid transporter 1 (LAT1) transports large neutral amino acids such as leucine, isoleucine, valine, phenylalanine, tyrosine, tryptophan, methionine, and histidine (27, 28). LAT1 requires covalent association with the heavy chain of 4F2 cell-surface antigen (4F2hc) for its functional expression in plasma membrane (27). Previous studies showed

Authors' Affiliations: Departments of [1]Medicine and Molecular Science, [2]Diagnostic Radiology and Nuclear Medicine, [3]Thoracic and Visceral Organ Surgery, [4]General Surgical Science, and [5]Tumor Pathology, Gunma University Graduate School of Medicine; [6]Gunma University School of Health Sciences, Showa-machi, Maebashi, Gunma, Japan; and [7]Department of Pharmacology and Toxicology, Kyorin University School of Medicine, Shinkawa, Mitaka, Tokyo, Japan

Received 5/25/07; revised 7/18/07; accepted 7/31/07.

The costs of publication of this article were defrayed in part by the payment of page charges. This article must therefore be hereby marked *advertisement* in accordance with 18 U.S.C. Section 1734 solely to indicate this fact.

Requests for reprints: Kyoichi Kaira, Department of Medicine and Molecular Science, Gunma University Graduate School of Medicine, Showa-machi, Maebashi, Gunma 371-8511, Japan. Phone: 81-27-220-8136; Fax: 81-27-220-8136; E-mail: kkaira1970@yahoo.co.jp.

doi:10.1158/1078-0432.CCR-07-1294

that LAT1 was highly expressed in proliferating tissues including tumor cell lines and primary human tumors (28, 29).

Based on these backgrounds, we have conducted a study to determine the relationship between LAT1 expression and [^{18}F]FMT uptake in patients with NSCLC. In this study, we examined the clinical usefulness of [^{18}F]FMT PET as compared with [^{18}F]FDG PET for diagnosing and staging NSCLC. We also investigated the relationship between LAT1 expression and Ki-67 labeling index (LI) as a proliferative marker of tumor cells.

Materials and Methods

Patients

Fifty-four patients with proven or suspected NSCLC were enrolled in the study that was conducted at the Gunma University Hospital, Japan,

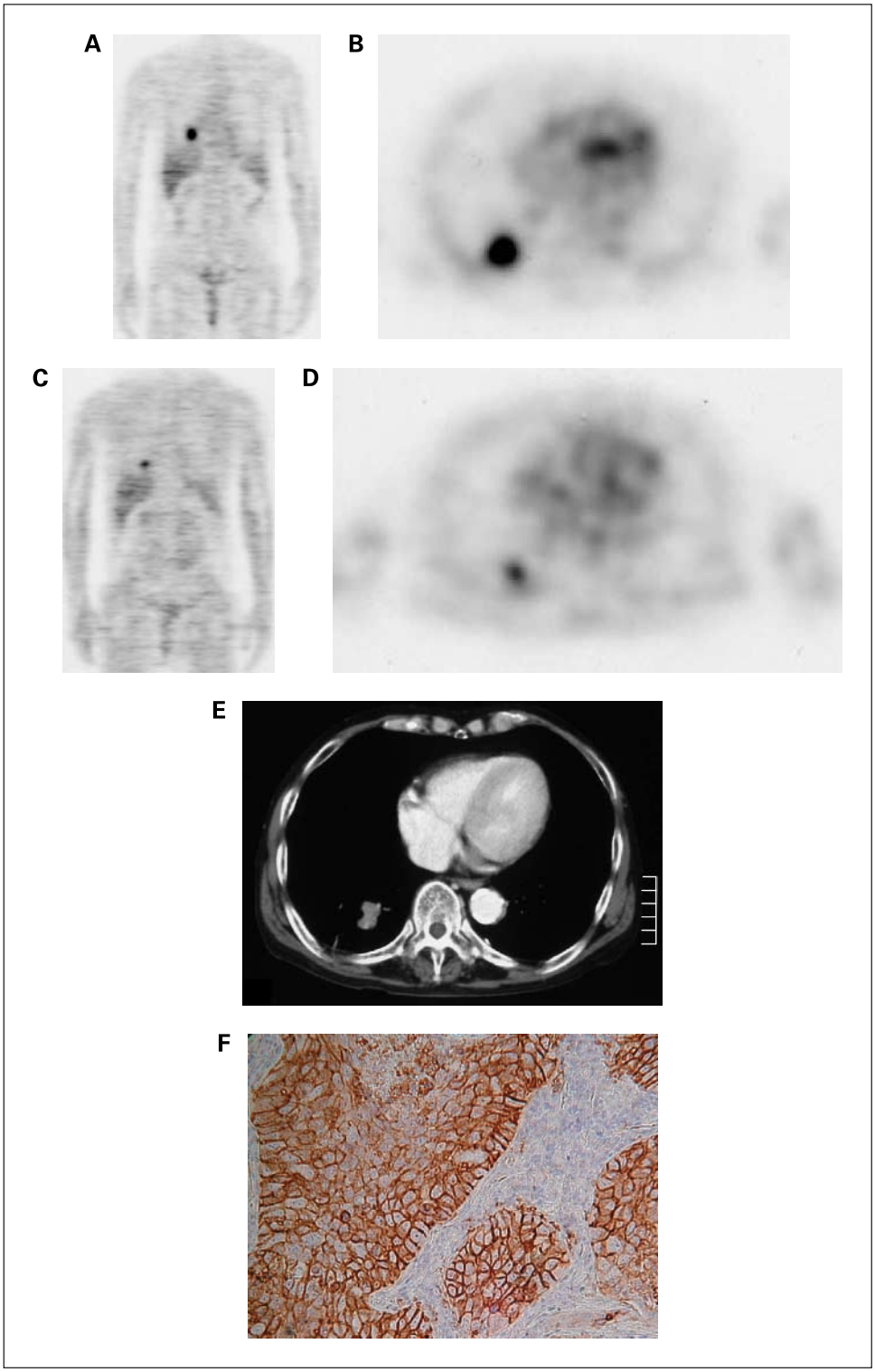

Fig. 1. Coronal (*A*) and transaxial (*B*) sections of [^{18}F]FDG PET of a 74-y-old man with LCC of the right lung (p-$T_2N_0M_0$). Tumoral [^{18}F]FDG uptake is intense with SUV of 6.00. Corresponding coronal (*C*) and transaxial (*D*) sections of ^{18}F-FMT also show intense tracer uptake (SUV, 2.66) in the lesion, which is depicted on CT scan (*E*). The scoring of LAT1 immunostaining was grade 4 and its immunostaining pattern was membranous (×400; *F*).

Table 1. Detectability of primary tumor on [^{18}F]FMT PET and [^{18}F]FDG PET according to the size of the tumor

Maximum diameter of primary tumor (mm)	[^{18}F]FMT PET		[^{18}F]FDG PET	
	Sensitivity	Maximal SUV	Sensitivity	Maximal SUV
10-20	7/12 (58.3%)	1.62 ± 0.81*	9/12 (75%)	5.46 ± 1.68 †
20-30	12/12 (100%)	1.23 ± 0.46*	12/12 (100%)	6.61 ± 2.33
>30	26/26 (100%)	1.64 ± 0.70*	26/26 (100%)	7.87 ± 2.94 †

*The difference among these three groups is not statistically significant. P = 0.88, 1.62 ± 0.81 versus 1.23 ± 0.46; P = 0.86, 1.62 ± 0.81 versus 1.64 ± 0.70; P = 0.11, 1.23 ± 0.46 versus 1.64 ± 0.70.
† Significant difference between these two groups (P = 0.03).

a teaching and tertiary care hospital and a major referral site for patients with cancer. All consecutive patients referred for surgery from November 2005 to January 2007 were included in the study. [^{18}F]FMT PET was done as part of preoperative workup. Patients also underwent [^{18}F]FDG PET, CT of the thorax, whole-body bone scanning for the detection of possible distant metastases, and bronchoscopy with the biopsy for diagnostic confirmation. Patients in whom findings on CT, [^{18}F]FDG PET, or both were consistent with stage N_3 disease also underwent diagnostic mediastinoscopy. Depending on the results of staging, patients then underwent either chemotherapy or surgical management. Staging was conducted in accordance with internationally accepted staging guidelines. Four patients were excluded for further studies because histologic analysis revealed small-cell carcinoma in two patients and the recurrence of breast cancer could not be completely ruled out in the other two patients. Thus, 50 patients (35 men and 15 women) with a mean age of 69 years (range, 42-82 years) were analyzed in the study. Histologic analysis revealed adenocarcinoma (AC) in 26 patients, squamous cell carcinoma (SQC) in 20, large cell carcinoma (LCC) in 2, and others in 2. All patients agreed to participate in these studies and provided written informed consent. The study protocol was approved by the institutional review board.

Surgery and staging

Lung resection was done with mediastinal lymph node dissection according to the mapping system of the American Thoracic Society (30). Sites of increased [^{18}F]FDG and [^{18}F]FMT uptake corresponding to primary tumors, lymph nodes, and distant disease sites were recorded. PET and clinical and pathologic tumor-node-metastasis (TNM) stages were established using the International System for Staging Lung Cancer adopted by the American Joint Committee on Cancer and the Union Internationale Centre le Cancer (30). Surgery was done in 38 patients, which consisted of lung resection and mediastinal lymphadenectomy in 34 patients, exploratory thoracotomy in 3, and wedge resection in 1. Wedge resection was done in one patient because of the limited lung function. Lymphadenectomy was not done in this patient because mediastinal lymph nodes were <5 mm on CT and [^{18}F]FDG PET was negative for lymph node involvement. Of the three patients who underwent only exploratory thoracotomy, two had pleural dissemination and one had infiltration of the aorta. In the remaining 12 patients, diagnostic staging and histologic confirmation of malignancy was done by means of mediastinoscopy, bronchoscopy, or both. These patients were excluded from surgery because the three patients had occult extrathoracic metastases, six patients had N_2 disease on TNM staging, and three patients had T_4 disease without chest wall or mediastinal invasion. Complete pathologic TNM staging was done in 34 patients and disease was classified as stage IA in 12 patients, stage IB in 7 patients, stage IIA in 1 patient, stage IIB in 5 patients, stage IIIA in 6 patients, and stage IIIB in 3 patients.

PET studies

[^{18}F]FMT was synthesized in our cyclotron facility according to the method developed by Tomiyoshi et al. (17). Radiochemical yield of [^{18}F]FMT was ~20% and radiochemical purity was ~99%. [^{18}F]FDG was also produced in our facility as previously described (31). The patients were fasted for at least 6 h before the PET studies. PET study was done using a whole-body PET scanner with $Bi_4Ge_3O_{12}$ crystals (SET 2400W; Shimadzu) with 59.5-cm transverse fields of view, which produced 63 image planes with a 3.123-mm interval between images. Transverse resolution at the center of the field of view was 4.2 mm full width half maximum.

Two-dimensional date acquisition was initiated 50 min after the injection of 4 to 5 MBq/kg of [^{18}F]FMT or 5 to 6 MBq/kg of [^{18}F]FDG as previously described (18). The image protocol was set to use a

Table 2. Results of quantitative measurement of [^{18}F]FMT and [^{18}F]FDG according to the histopathologic subtypes of NSCLC

	Size, mm (range)	P	Maximal SUV				Sensitivity			
			[^{18}F]FMT		[^{18}F]FDG		[^{18}F]FMT		^{18}F-FDG	
			Range	P	Range	P	%	P	%	P
AC (n = 28)	28.6 ± 1.8 (12-55)		1.24 ± 0.51 (0.81-2.62)		6.03 ± 2.74 (1.30-13.2)		21/26 (80.7)		23/26 (88.5)	
		<0.001		<0.001		0.11		<0.05		0.17
SQC (n = 18)	37.1 ± 2.3 (15-99)		1.96 ± 0.70 (0.84-3.60)		7.46 ± 2.92 (2.71-13.3)		20/20 (100)		20/20 (100)	
		<0.001		<0.001		0.07		<0.05		0.13
Non-AC (n = 22)	38.5 ± 2.2 (15-99)		1.86 ± 0.68 (0.84-3.60)		7.69 ± 3.35 (2.71-15.6)		24/24 (100)		24/24 (100)	

Abbreviation: Non-AC, non–small-cell lung carcinoma except for adenocarcinoma.

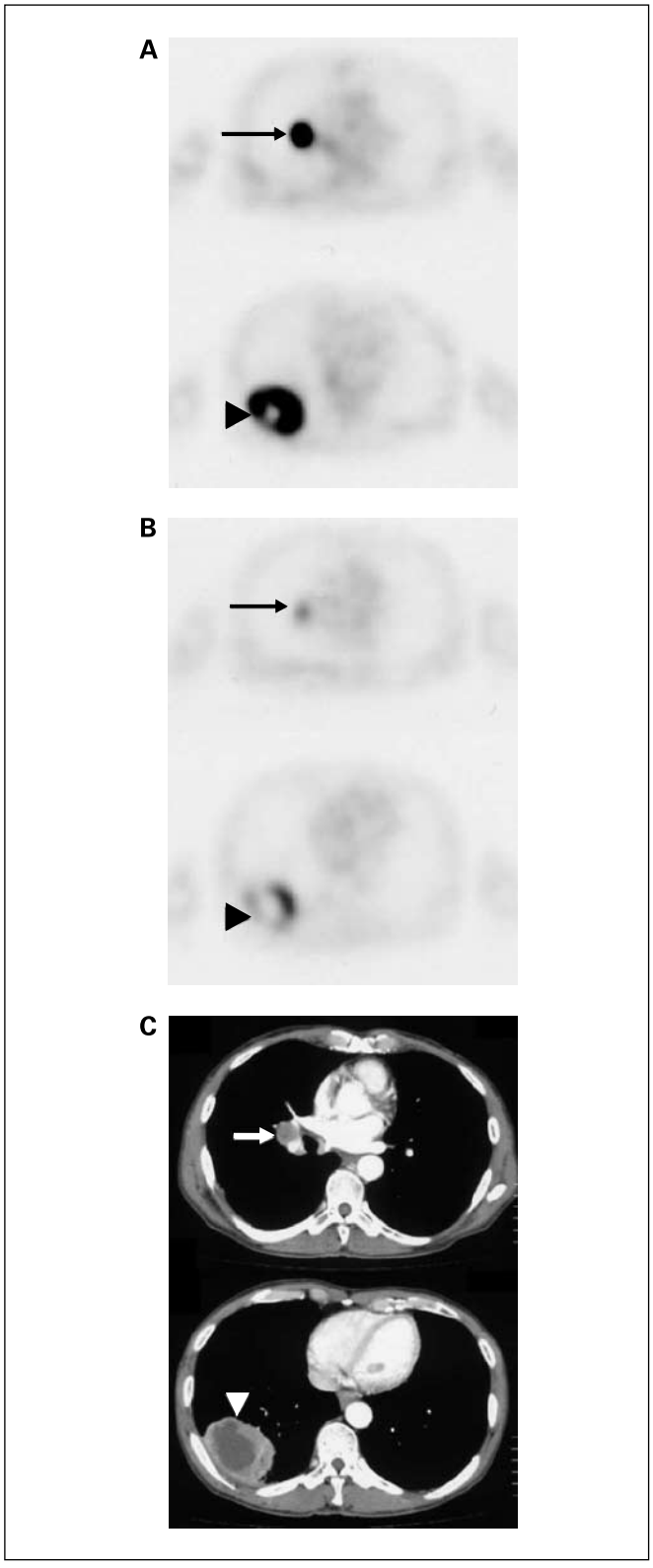

Fig. 2. [^{18}F]FDG PET (transaxial section; *A*), ^{18}F-FMT PET (transaxial section; *B*), and CT scans (*C*) of a 69-y-old man with SQC of the right lung (p-$T_2N_1M_0$). [^{18}F]FDG PET shows increased uptake of [^{18}F]FDG by the right hilar lymph node (SUV, 8.00; *arrow*) and primary tumor (SUV, 10.6; *arrowhead*). ^{18}F-FMT PET also shows increased uptake of ^{18}F-FMT by the right hilar lymph node (SUV, 1.59; *arrow*) and primary tumor (SUV, 2.69; *arrowhead*). CT reveals that [^{18}F]FDG and ^{18}F-FMT uptake in the lesions corresponds to the right hilar lymph node (*arrow*) and the primary tumor (*arrowhead*).

simultaneous emission-transmission method with a rotating external source (370 MBq of ^{68}Ge-^{68}Ga at the time of installation) and to acquire 4 to 10 bed positions (8-min acquisition per bed position) according to the range of imaging. In cases of bone and skin lesions, a maximum of 10 bed positions was acquired to cover the whole body. Attenuation-corrected transverse images obtained with [^{18}F]FMT and [^{18}F]FDG were reconstructed with the ordered-subsets expectation maximization algorithm into 128 × 128 matrices with pixel dimensions of 4.0 mm in-plane and 3.125 mm axially. Coronal images with a 9.8-mm section thickness were also reconstructed from attenuation-corrected transverse images for visual interpretation.

Data analysis

All [^{18}F]FDG and [^{18}F]FMT PET images were interpreted by two experienced nuclear physicians. The interpreting physicians were unaware of the patient's clinical history and data. Moderate uptake and intense uptake were defined as positive results of visual interpretation; faint uptake and no uptake, which were less than the uptake in the normal mediastinum, were defined as negative results. Discrepant results were resolved by the consensus review. For the semiquantitative analysis, functional images of the standardized uptake value (SUV) were produced using attenuation-corrected transaxial images, injected doses of [^{18}F]FMT and [^{18}F]FDG, patient's body weight, and the cross-calibration factor between PET and dose calibrator (32). SUV was defined as follows:

$$\text{SUV} = \text{radioactive concentration in the region of interest (MBq/g)} / \text{injected dose (MBq)} / \text{patient's body weight (g)}.$$

Regions of interest of ~1-cm diameter were manually drawn on the SUV images over the area corresponding to the maximal tracer uptake in the lesions, when multiple lesions were present or the lesion was >1 cm in diameter. SUV of background was defined by drawing region of interest at the site other than lymphadenopathy in the mediastinum. When the lesion showed no significant tracer uptake, region of interest was placed retrospectively on the PET image with reference to the CT image. Region of interest analysis was conducted by a nuclear physician with the aid of corresponding CT scans. The maximal SUV in the region of interest was used as a representative value for the assessment of [^{18}F]FMT and [^{18}F]FDG uptake in the lesion.

Immunohistochemical staining with LAT1 and Ki-67

LAT1. LAT1 expression was determined by immunohistochemical staining with an affinity-purified polyclonal rabbit anti-human LAT1 antibody (28). An oligopeptide corresponding to amino acid residues 497 to 507 of human LAT1 (CQKLMQVVPQET) was synthesized. The NH_2-terminal cysteine residue was introduced for conjugation with keyhole limpet hemocyanin. Antipeptide antibody was produced as described elsewhere (33). For immunohistochemical analysis, antiserum was affinity purified as previously described (33).

Immunohistochemical staining was done on paraffin sections using a polymer peroxidase method (Envision +/horseradish peroxidase; DakoCytomation). Briefly, deparaffinized, rehydrated sections were treated with 0.3% hydrogen peroxide in methanol for 30 min to block endogenous peroxidase activity. To expose antigens, sections were autoclaved in 10 mmol/L sodium citrate buffer (pH 6.0) for 5 min and cooled for 30 min. After rinsing in 0.05 mol/L TBS containing 0.1% Tween 20, the sections were incubated with affinity-purified anti-LAT1 antibody (1.2 mg/mL; 1:3,200) overnight at 4°C. Thereafter, they were incubated with Envision (+) rabbit peroxidase (DAKO) for 30 min. The peroxidase reaction was done using 0.02% 3,3′-diaminobenzidine tetrahydrochloride and 0.01% hydrogen peroxide in 0.05 mol/L Tris-HCl buffer (pH 7.4). Finally, nuclear counterstaining was done with Mayer's hematoxylin. For negative control, incubation step with the primary antibody was omitted. The specificity of immunoreactions using the anti-LAT1 antibody was established in previous studies (29, 34).

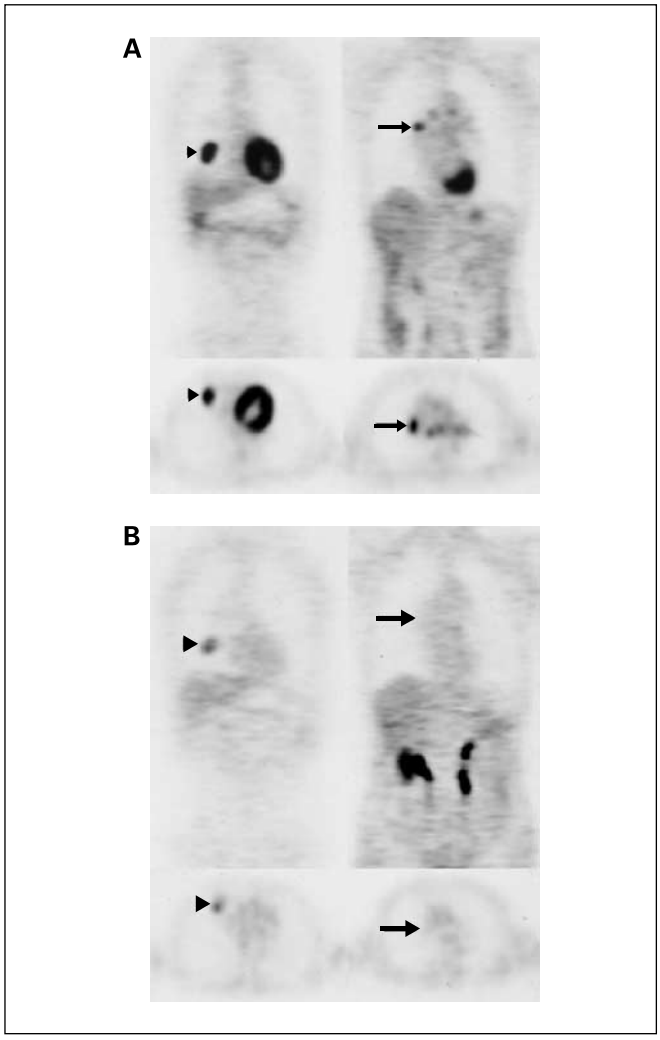

Fig. 3. Coronal and transaxial section of [^{18}F]FDG PET and ^{18}F-FMT PET of a 69-y-old man with SQC of the right lung (p-$T_1N_0M_0$). *A,* [^{18}F]FDG PET shows increased uptake of [^{18}F]FDG by the right hilar lymph node (SUV, 3.47; *arrow*) and primary tumor (SUV, 5.37; *arrowhead*). *B,* ^{18}F-FMT PET also shows increased uptake of ^{18}F-FMT by the primary tumor (SUV, 2.27; *arrowhead*). However, ^{18}F-FMT PET shows no increased uptake in the lesions corresponding to the right hilar lymph node (*arrow*). Thoracotomy was done, and histologic examination revealed no evidence of lymph node metastasis.

LAT1 expression was considered positive only if distinct membrane staining was present. Staining intensity was scored as follows: 1, <10% of tumor area stained; 2, 11% to 25% stained; 3, 26% to 50% stained; and 4, ≥51% stained. The tumors in which stained tumor cells made up >25% of the tumor were graded as positive. According to this scoring protocol, two investigators from the authors, who have no prior knowledge of the clinical data, independently graded the staining intensity in all cases. To test the interobserver variability, each section was reassessed by the same investigators after the first assessment had been completed. The time interval between the first and second assessments was at least 4 weeks. The intraobserver variability was also determined by comparing the values of the first measurements of two investigators.

Ki-67. The detailed protocol for immunostaining was published elsewhere (35). Briefly, formalin-fixed and paraffin-embedded sections of resected specimens were dewaxed, rehydrated, and boiled in 0.01 mol/L citrate buffer for 20 min. For immunostaining, the monoclonal murine antibody MIB-1 (DAKO), specific for human nuclear antigen Ki-67, was used in a 1:40 dilution. The sections were lightly counterstained with hematoxylin. Sections of a normal tonsil were used as positive control for proliferating cells.

A highly cellular area of the immunostained sections was evaluated. All epithelial cells with nuclear staining of any intensity were defined as positive. Approximately 1,000 nuclei were counted on each slide. Proliferative activity was assessed as the percentage of MIB-1–stained nuclei (Ki-67 LI) in the sample. Sections were evaluated by two investigators separately; in case of discrepancies, both would evaluate the slide simultaneously and would agree in their final assessment. Neither investigator had knowledge of patient outcome.

Statistical analysis. Data are presented as mean, range, and SD. The relationship between SUVs of [^{18}F]FMT and those of [^{18}F]FDG in the lesions was assessed by linear regression analysis. $P < 0.05$ indicated a statistically significant difference. Fisher's exact test was used to examine the association of two categorical variables. Correlation between maximal SUV and the levels of immunohistochemical staining of LAT1 or Ki-67 was analyzed using the nonparametric Spearman's rank test. Statistical analysis was done using StatView J-4.5 for Macintosh.

Results

Primary tumor status. [^{18}F]FMT PET showed visible tracer uptake in 45 of 50 (90.0%) primary tumors. The SUV of [^{18}F]FMT ranged from 0.81 to 3.60 (mean, 1.51 ± 0.61). As for [^{18}F]FDG PET, visible tracer uptake was detected in 47 of 50 (94.0%) primary tumors. The SUV of [^{18}F]FDG ranged from 1.30 to 15.6 (mean, 6.81 ± 3.13). The maximal SUV of [^{18}F]FDG of primary tumor was significantly higher than that of [^{18}F]FMT ($P < 0.001$). However, the sensitivity of [^{18}F]FDG PET for detecting primary tumor was not significantly higher than that of [^{18}F]FMT PET ($P = 0.35$). Moreover, the SUV of [^{18}F]FMT (mean, 1.51 ± 0.61) was significantly higher than that of background (mean, 0.67 ± 0.14) in the mediastinum ($P < 0.001$). Images of [^{18}F]FDG PET and [^{18}F]FMT PET are shown in Fig. 1.

We divided patients into three groups according to the maximum tumor diameter (10-20, >20-30, and >30 mm) and compared the sensitivity of [^{18}F]FMT PET and [^{18}F]FDG PET for detecting primary tumor among three groups (Table 1). [^{18}F]FMT PET and [^{18}F]FDG PET showed visible tracer uptake in all of 38 primary tumors with a maximum diameter of

Table 3. Efficacy of [^{18}F]FMT PET and [^{18}F]FDG PET in detecting malignant lymph nodes

	Sensitivity (%)	Specificity (%)	Accuracy (%)	Positive predictive value (%)	Negative predictive value (%)
[^{18}F]FMT PET	57.8	100	92.5	100	91.7
[^{18}F]FDG PET	65.7	91.0	86.5	60.9	92.5
P	0.31	<0.001	0.058	0.002	0.92

Table 4. Performance of [^{18}F]FDG and [^{18}F]FMT PET for detection of lymph node metastases

	Sensitivity			Specificity		
	[^{18}F]FMT (%)	[^{18}F]FDG (%)	*P*	[^{18}F]FMT (%)	[^{18}F]FDG (%)	*P*
AC	16/28 (57.1)	19/28 (67.8)	0.17	72/72 (100)	68/72 (94.4)	0.059
SQC	6/9 (66.7)	6/9 (66.7)	0.69	96/96 (100)	86/96 (89.4)	<0.001
Non-AC	6/10 (60.0)	6/10 (60.0)	0.68	106/106 (100)	94/106 (88.6)	<0.001

>20 mm. However, the false-negative [^{18}F]FMT PET findings occurred in 5 of 12 primary tumors with a maximum diameter of <20 mm. The five false-negative [^{18}F]FMT PET findings occurred in pure bronchioloalveolar carcinoma (n = 4) and AC with prominent bronchioloalveolar features (n = 1). [^{18}F]FDG PET findings were false-negative in three of the five lesions. Moreover, we compared the maximal SUVs of [^{18}F]FMT PET and [^{18}F]FDG PET among these three groups (Table 1). The difference in the maximal SUVs of [^{18}F]FMT among these three groups was not statistically significant, whereas the difference in the maximal SUVs of [^{18}F]FDG was statistically significant between 10-20 mm and >30 mm (P = 0.03).

We evaluated the accumulation of [^{18}F]FMT and [^{18}F]FDG in the primary tumors according to the histopathologic subtypes of NSCLC (Table 2). The tumor size of the AC ranged from 12 to 55 mm (mean, 28.6 ± 1.8 mm), whereas the tumor size of SQC ranged from 15 to 99 mm (mean, 37.1 ± 2.3 mm), which was significantly larger than that of the AC (P < 0.001). In the imaging of [^{18}F]FMT, the maximal SUV (P < 0.001) and sensitivity (P < 0.05) for SQC was significantly higher than that for AC. The difference was also noted when comparing the same size of SQC and AC tumors (data not shown). In contrast, [^{18}F]FDG PET showed no significant difference in the SUV or sensitivity between them.

Lymph node status. In 216 regions of resected or sampled lymph nodes, 38 were positive and 178 were negative based on the histologic analysis as a reference (Fig. 2). The sensitivity of [^{18}F]FMT PET for detecting malignant lymph nodes was 22 of 38 (57.8%) lesions, with a specificity of 100% (178 of 178 lesions) and an accuracy of 92.5% (200 of 216 lesions). The sensitivity, specificity, and accuracy of [^{18}F]FDG PET were 65.7% (25 of 38 lesions), 91.0% (162 of 178 lesions), and 86.5% (187 of 216 lesions), respectively. The false-positive lymph nodes were observed on [^{18}F]FDG PET in 16 lesions [sarcoidosis (n = 4), silicosis (n = 3), and inflammatory change (n = 9); Fig. 3]. The difference in accuracy and sensitivity of [^{18}F]FDG and [^{18}F]FMT in disease detection did not reach statistical significance (P = 0.058 and P = 0.31, respectively). However, the specificity of [^{18}F]FMT was significantly higher than that of [^{18}F]FDG (P < 0.001; Table 3). In contrast, SUV of [^{18}F]FMT (1.27 ± 0.38) was lower than that of [^{18}F]FDG (5.82 ± 3.50; P < 0.001).

We compared the lymph node staging with [^{18}F]FMT and that with [^{18}F]FDG PET and evaluated them according to the histopathologic subtypes of NSCLC (Table 4). The sensitivity of [^{18}F]FMT PET was inferior to that of [^{18}F]FDG PET in patients with AC, although there was no significant difference. For the patients with SQC and non-AC, however, the sensitivity of [^{18}F]FMT PET was similar to that of [^{18}F]FDG PET. The specificity, accuracy, and positive predictive value of [^{18}F]FMT were significantly higher than those of [^{18}F]FDG in patients with SQC and non-AC.

Metastasis status. In 3 of 50 (6.0%) patients, [^{18}F]FDG and [^{18}F]FMT PET detected unsuspected extrathoracic focal abnormalities suggestive of metastases. Of the four extrapulmonary malignant lesions sampled, three lesions (axillary lymph node, cervical lymph node, and bone) were detected by both [^{18}F]FDG PET and [^{18}F]FMT PET. The other lesion (skin) was detected only by [^{18}F]FDG PET.

Patient-based analysis and staging. Of the 34 patients with complete pathologic TNM staging, [^{18}F]FMT PET correctly indicated the staging in 23 (67.6%) patients, and [^{18}F]FDG PET correctly indicated the staging in 21 (61.7%) patients (P = 0.78). [^{18}F]FMT PET understaged 11 (32.4%) patients and overstaged no patient (0%), whereas [^{18}F]FDG PET understaged 6 (17.6%) patients and overstaged 8 (23.5%) patients. [^{18}F]FMT PET incorrectly indicated 5 patients as disease-free and 6 patients as false-negatives for lymph nodes. [^{18}F]FDG PET incorrectly indicated 3 patient as disease-free, 6 patients with false-positive lymph nodes, and 4 patients with false-negative lymph nodes.

Immunohistochemical analysis for LAT1 and Ki-67. LAT1 and Ki-67 immunohistochemical stainings were evaluated for the 34 primary tumor specimens of 34 patients with complete pathologic TNM staging (Table 5). Of the 34 patients (21 men and 13 women; mean age, 69 years; range, 42-80 years), 16 patients had AC, 16 patients had SQC, and 2 patients had LCC. LAT1 immunostaining was detected in carcinoma cells in tumor tissues and localized predominantly on their plasma membrane (Fig. 1F). All positive cells revealed strong membranous LAT1 immunostaining. It is noted that the staining intensity of the cell membrane and the percentage of positive cells were considerably greater in SQC and LCC than AC. The cytoplasmic staining was rarely evident. A positive LAT1 expression was recognized in 76.5% of primary tumors [26 of 34 lesions; 50% of AC (8 of 16 lesions), 100% of SQC (16 of 16 lesions), and 100% of LCC (2 of 2 lesions)]. The incidence of a positive LAT1 expression was significantly different between AC and SQC and between AC and non-AC (P < 0.001 and P < 0.001, respectively). The average score of the LAT1 expression was 2.9 ± 1.1 on a scale of 1 to 4. The LAT1 score was 2.3 ± 1.0 in AC, 3.5 ± 0.6 in SQC, and 4.0 ± 0.0 in LCC. There was a significant difference between AC and SQC in the LAT1 score (P < 0.001). LAT1 expression was not detected in 11.7% of primary tumors [4 of 34 lesions; 25% of AC (4 of 16 lesions)]. Of the four primary tumors with negative LAT1 expression, [^{18}F]FMT PET showed no uptake in all cases (100%), whereas [^{18}F]FDG PET showed no uptake in one case (25%). Moreover, we investigated the correlation between LAT1 expression and pathologic features (pleural involvement, lymphatic permeation,

Table 4. Performance of [^{18}F]FDG and [^{18}F]FMT PET for detection of lymph node metastases (Cont'd)

Positive predictive value			Negative predictive value			Accuracy		
[^{18}F]FMT (%)	[^{18}F]FDG (%)	*P*	[^{18}F]FMT (%)	[^{18}F]FDG (%)	*P*	[^{18}F]FMT (%)	[^{18}F]FDG (%)	*P*
16/16 (100)	19/23 (82.6)	0.11	72/84 (85.7)	68/77 (88.3)	0.42	88/100 (88.0)	87/100 (87.0)	0.50
6/6 (100)	6/13 (46.1)	0.03	96/99 (97.0)	89/92 (96.7)	0.62	102/105 (97.1)	95/105 (90.5)	0.04
6/6 (100)	6/18 (33.3)	<0.001	106/110 (96.4)	94/98 (95.9)	0.57	112/116 (96.6)	100/116 (86.2)	0.004

vascular invasion, and lymph node metastasis). However, no significant difference was found between LAT1 expression positive (n = 26) and negative (n = 8) groups in these pathologic features.

The Ki-67 LI averaged 55 ± 23% (median, 55%) and ranged from 14% to 92% for the 34 lesions. The Ki-67 LI was 40 ± 18% (median, 39%) in AC, 66 ± 20% (median, 72%) in SQC, and 69 ± 27% in LCC. The Ki-67 LI was significantly different between AC and SQC ($P < 0.001$).

Correlation between maximal SUV, LAT1, and Ki-67. Significant correlation was found between LAT1 expression and maximal SUVs of [^{18}F]FMT (Spearman's rank correlation coefficient $\rho = 0.890$, $P < 0.001$), between Ki-67 and maximal SUVs of [^{18}F]FMT ($\rho = 0.566$, $P = 0.0014$), and between LAT1 and Ki-67 ($\rho = 0.651$, $P < 0.001$). Significant correlation was also found between LAT1 and maximal SUVs of [^{18}F]FDG (Spearman's rank correlation coefficient $\rho = 0.657$, $P < 0.001$) and between Ki-67 and maximal SUVs of [^{18}F]FDG ($\rho = 0.519$, $P = 0.003$; Fig. 4). No significant correlation was found between maximal SUVs of [^{18}F]FMT and maximum tumor diameter ($\rho = 0.321$, $P = 0.695$) or between Ki-67 and maximum tumor diameter ($\rho = 0.302$, $P = 0.872$). Slightly positive correlation was found between LAT1 and maximum tumor diameter ($\rho = 0.363$, $P = 0.04$).

Discussion

This is the first study to evaluate the diagnostic usefulness of [^{18}F]FMT PET in comparison with [^{18}F]FDG PET in patients with NSCLC. [^{18}F]FMT PET is a noninvasive procedure to detect malignant lesions and has high diagnostic yield. This method has no false-positive findings in the present study and could improve the specificity to detect both primary tumor and lymph node metastasis. Uptake of the tracer correlates with overexpression of LAT1 in NSCLC.

The sensitivity of [^{18}F]FMT PET in depicting malignant lesions seems to be lower than that of [^{18}F]FDG PET; however, the difference was not statistically significant. In contrast, the specificity and positive predictive value of [^{18}F]FMT PET were significantly superior to those of [^{18}F]FDG PET. Previous studies revealed that [^{18}F]FDG PET suffers from false-positives in sarcoidosis, silicosis, and inflammatory changes due to abnormal [^{18}F]FDG uptake, whereas [^{18}F]FMT PET showed no false-positive uptake in the lymph nodes. Because no [^{18}F]FMT uptake was detected in the sarcoid lesions, [^{18}F]FMT PET in combination with [^{18}F]FDG PET was regarded useful in distinguishing lung cancers from sarcoidosis (23, 36). In the previous study, SUVs of [^{18}F]FMT represented a statistical difference between lung cancer (1.30 ± 0.54) and sarcoidosis (0.77 ± 0.24; $P < 0.001$). The sarcoid lesions were positive on [^{18}F]FDG PET and were negative on [^{18}F]FMT PET in all patients (36).

We found the differential accumulation of [^{18}F]FMT in different histopathologic subtypes of NSCLC. In the imaging of primary tumors, the maximal uptake of [^{18}F]FMT and the sensitivity of [^{18}F]FMT PET in SQC and LCC were significantly higher than those in AC, whereas [^{18}F]FDG PET showed no significant difference between them. The sensitivity of [^{18}F]FMT PET in depicting malignant lesions was similar to that of [^{18}F]FDG PET in patients with SQC or LCC. However, there was a limitation of [^{18}F]FMT PET in AC with prominent bronchioloalveolar features and with a maximum tumor diameter <20 mm.

A large number of studies have been conducted to evaluate the usefulness of [^{18}F]FDG PET in the diagnosis of NSCLC, and meta-analysis revealed that a sensitivity of 96% and a specificity of 80% were obtained (16, 37). However, the major problem in using [^{18}F]FDG PET is that an increased uptake of [^{18}F]FDG is observed in both malignant tumors and inflammatory lesions (38). In search of more selective tracers for PET imaging, a

Table 5. LAT1 expression and Ki-67 LI of the tumor according to the histopathologic subtypes of NSCLC

	No. lesions	LAT1 expression		Ki-67 LI (%)
		Positive rate	Score	
AC	16	8/16 (50.0%)*	2.3 ± 1.0 †	40 ± 18 (14-72) ‡
SQC	16	16/16 (100%)*	3.5 ± 0.6 †	66 ± 20 (26-92) ‡
LCC	2	2/2 (100%)	4.0, 4.0	50, 88
ALL	34	26/34 (76.5%)	2.9 ± 1.1	55 ± 23 (14-92)

*Significant difference between AC and SQC ($P < 0.001$).
† Significant difference between AC and SQC ($P < 0.001$).
‡ Significant difference between AC and SQC ($P = 0.003$).

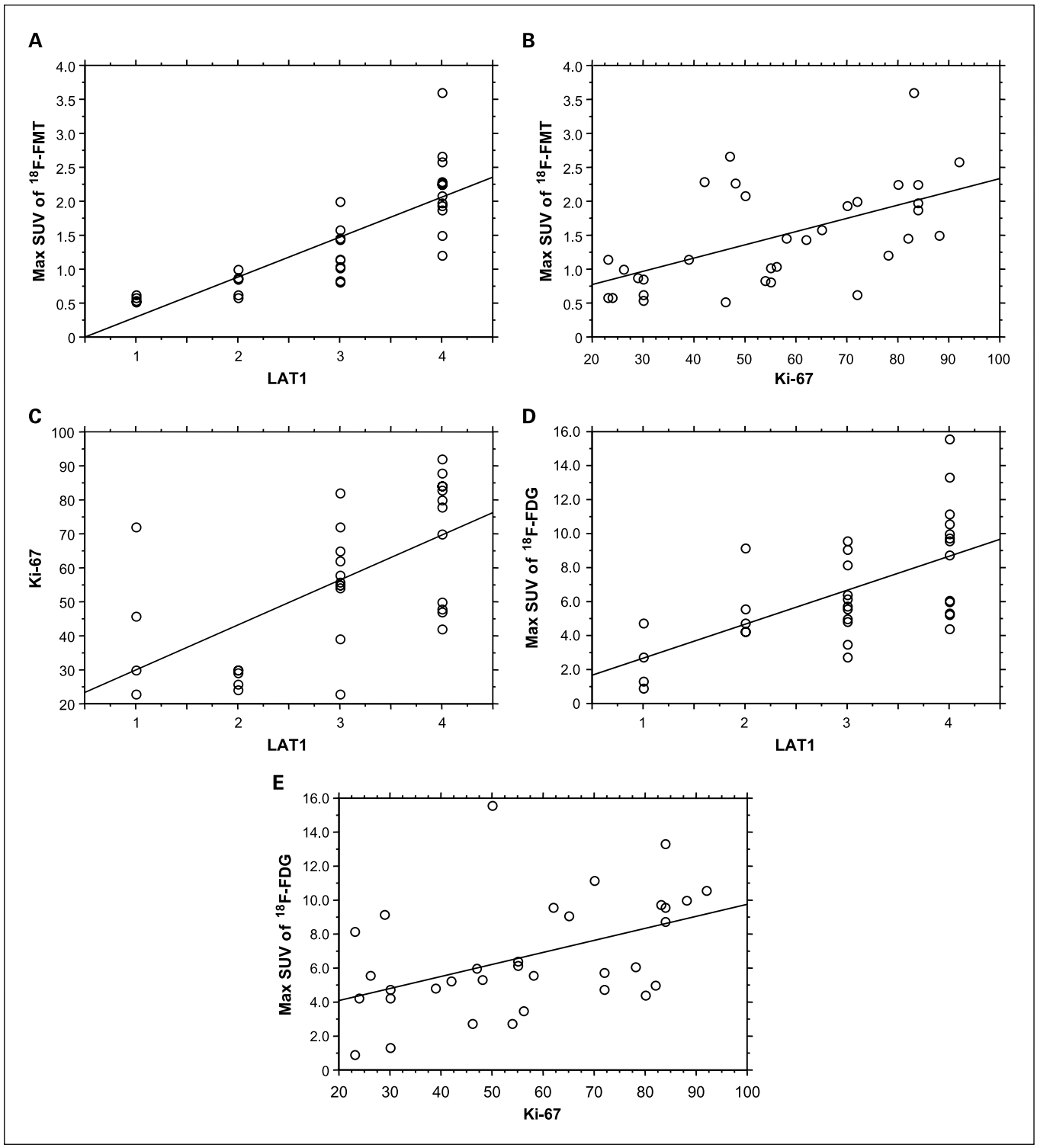

Fig. 4. Correlation between immunohistochemical analysis and PET with ^{18}F-FMT and [^{18}F]FDG. Significant correlation is observed between LAT1 and ^{18}F-FMT SUV_{max} ($\rho = 0.890$, $P < 0.001$; *A*), Ki-67 and ^{18}F-FMT SUV_{max} ($\rho = 0.566$, $P = 0.0014$; *B*), Ki-67 and LAT1 ($\rho = 0.651$, $P < 0.001$; *C*), LAT1 and [^{18}F]FDG SUV_{max} ($\rho = 0.657$, $P < 0.001$; 0.001; *D*), and Ki-67 and [^{18}F]FDG SUV_{max} ($\rho = 0.519$, $P = 0.003$; *E*).

number of PET ligands have been investigated (13–15). There are several clinical studies obtained with other tyrosine derivatives such as 2-^{18}F-fluoro-L-tyrosine ([^{18}F]FET) and 3-^{123}I-iodo-α-methyl-L-tyrosine (^{123}I-IMT; refs. 39–41). Pauleit et al. (40) investigated the diagnostic potential of [^{18}F]FET in the imaging of lung cancer. In their study, all SQCs were found to be [^{18}F]FET positive, whereas most ACs were found to be [^{18}F]FET negative. Compared with [^{18}F]FDG, [^{18}F]FET PET may

allow a better distinction between tumors and inflammatory tissues in patients with SQC; however, [^{18}F]FET PET seems not to be a useful method to diagnose NSCLC because [^{18}F]FET PET shows no uptake in most ACs. Although tumor [^{18}F]FMT uptake may be lower than [^{18}F]FET, background activity seems to be lower than [^{18}F]FET. However, we could not compare the uptake of [^{18}F]FMT with that of [^{18}F]FET because SUV of [^{18}F]FET in lung cancer and background has not been provided (40). Whereas, ^{123}I-IMT single-photon emission computed tomography has a high sensitivity for the detection of primary tumors of NSCLC (sensitivity, 94%), but it is not useful for small metastases (<2 cm in diameter; ref. 41). Experiments with *Xenopus* oocytes showed that the radioiodinated tyrosine derivative ^{123}I-IMT was selectively transported via the human LAT1 (42). However, several observations suggest that [^{18}F]FET may be selectively transported via LAT2, which is expressed in normal cells (40). The synthetic leucine amino acid analogue anti–1-amino-3-^{18}F-fluorocyclobutane-1-carboxylic acid (anti-[^{18}F]FACBC) has been reported to be a ligand that permits the evaluation of the L-type amino acid transporter system (43). [^{18}F]FACBC may prove useful for imaging brain and pelvic tumors because of its low uptake within the brain and the urinary bladder. However, there are no clinical studies on [^{18}F]FACBC with PET in NSCLC. Radiochemical yield of [^{18}F]FMT is lower than [^{18}F]FET and is equivalent to FACBC (17). The low yield of [^{18}F]FMT may not allow the delivery of large amount to the hospitals without on-site cyclotron as far as the present apparatus and procedure are used.

For patients with pulmonary tumors, our data showed a highly significant correlation between tumoral uptake of [^{18}F]FMT and level of LAT1 expression. The level of LAT1 expression varied in association with histologic malignancy of NSCLC. The expression in SQC and LCC was significantly higher than that in AC. Uptake of [^{18}F]FMT was also higher in SQC and LCC than in AC. A previous study showed that Glut1 expression and [^{18}F]FDG uptake were correlated with histologic malignancy of NSCLC (36) and the expression of Glut1 was higher in SQC than in AC (36). Clinically, [^{18}F]FDG uptake was also higher in SQC and LCC than in AC. LAT1 is the amino acid transporter expressed in NSCLC and is specific to malignant tumors. However, the possible factors to determine the [^{18}F]FMT accumulation in lung cancers need to be studied as well.

It is widely known that amino acid transport systems play an important role in the regulation of cellular proliferation, whereas the details of its function to promote tumor cell proliferation have not been clarified (27). LAT1 expression is up-regulated in both tumor cells and established tumor cell lines. LAT1 seems to supply the cells with sufficient amount of essential amino acids to support their rapid proliferation. LAT1 mRNA was detected at high level in T24 bladder carcinoma cells, RERF-LC-MA lung small-cell carcinoma cells, and HeLa uterine cervical carcinoma cells (28). Nakanishi et al. (44) investigated the LAT1 expression in normal lung, atypical adenomatous hyperplasia, and AC of the lung. They found that the incidence of a positive expression for LAT1 protein was inversely correlated with the differentiation from low-grade atypical adenomatous hyperplasia to AC (44). Furthermore, LAT1 protein overexpression in atypical adenomatous hyperplasia and AC showed a significant association with the Ki-67 LI, indicating an up-regulation of metabolic activity (44). In our study, Ki-67 LI is significantly correlated with LAT1 expression and with [^{18}F]FMT uptake. LAT1 expression shows a significant association with tumor cell proliferation. The correlation between Ki-67 expression and [^{18}F]FDG uptake has been reported elsewhere (45, 46). A significant correlation between [^{18}F]FDG uptake and proliferative activity was found for NSCLC (46, 47). Our results also show that there is a significant correlation between [^{18}F]FMT uptake and proliferative activity. The correlation between Ki-67 expression and PET tracer uptake tended to be higher in [^{18}F]FMT than in [^{18}F]FDG. However, the low correlation coefficient may be because of the contribution of other factors in cellular proliferation as discussed above.

In human neoplasms, the association between LAT1 expression and clinical features of the tumors is unclear. Kobayashi et al. (48) described that LAT1 expression in esophageal carcinoma was higher in cancerous tissue than in noncancerous tissue, and the expression increased in relation to depth of invasion, maximum tumor diameter, and differentiation. In our study, LAT1 expression did not increase in connection with pleural involvement, lymphatic permeation, vascular invasion, or lymph node metastasis. Although the low correlation was found between LAT1 expression and maximum tumor diameter, there was no significant correlation between [^{18}F]FMT uptake and maximum tumor diameter. No clinicopathologic study of LAT1 expression has been reported in patients with lung cancer. Because our sample size is small, a large-scale study would be conducted to acquire evidence for the clinicopathologic features in LAT1 expression.

One of the limitations of our study is the lack of a group of patients with tumors <10 mm in size. Another limitation is that our study was not evaluated with the latest PET-CT apparatus for the staging of NSCLC patients. There is a report stating that the staging of NSCLC is significantly accurate with integrated PET-CT machine as compared with dedicated PET machine (5). A further limitation is that we did not investigate the possible link between the overexpression of LAT1 and that of 4F2hc known to be required for the functional expression of LAT1 (27). It was previously reported that overexpression of 4F2hc induces cell proliferation (26, 49). Thus, the study of the correlation between 4F2hc expression and [^{18}F]FMT uptake may provide an additional insight into the interpretation of [^{18}F]FMT PET.

Conclusion

In the present study, the specificity for diagnosing lymph node involvement was higher by [^{18}F]FMT PET than [^{18}F]FDG PET. The uptake of [^{18}F]FMT was closely correlated with LAT1 expression. In patients with NSCLC, LAT1 expression in SQC and LCC was significantly higher than that in AC, which is corresponding to the higher [^{18}F]FMT uptake in patients with SQC and LCC as compared with AC. Further studies are warranted to verify the clinical implication of LAT1 expression as determined by [^{18}F]FMT PET in terms of clinical outcome in various histologies of NSCLC.

Acknowledgments

We thank T. Hikino and F. Hara for technical assistance in the immunohistochemical staining of LAT1 and Ki-67, and Drs. H. Aoki, T. Nakano, S. Kakegawa, and H. Endou for assistance with patient studies and data analysis.

References

1. Ettinger DS. Overview and state of the art in the management of lung cancer. Oncology (Huntingt) 2004; 18:3–9.
2. Mcloud TC, Bourgouin PM, Greenberg RW, et al. Bronchogenic carcinoma: analysis of staging in the mediastinum with CT by correlative lymph node mapping and sampling. Radiology 1992;182:319–23.
3. Shim SS, Lee KS, Kim BT, et al. Non-small cell lung cancer: prospective comparison of integrated FDG PET/CT and CT alone for preoperative staging. Radiology 2005;236:1011–9.
4. Pieterman RM, van Putten JW, Meuzelaar JJ, et al. Preoperative staging of non-small-cell lung cancer with positron-emission tomography. N Engl J Med 2000;343:254–61.
5. Lardinois D, Weder W, Hany TF, et al. Staging of non-small-cell lung cancer with integrated positron-emission tomography and computed tomography. N Engl J Med 2003;348:2500–7.
6. Vansteenkiste JF, Stroobants SG, De Leyn PR, et al. Lymph node staging in non-small-cell lung cancer with FDG-PET scan: a prospective study on 690 lymph node stations from 68 patients. J Clin Oncol 1998;16:2142–9.
7. Brock CS, Meikle SR, Price P. Dose fluorine-18 fluorodexyglucose metabolic imaging of tumor benefit oncology? Eur J Nucl Med 1997;24:691–705.
8. Hoffman JM, Waskin HA, Schifter T, et al. The use of FDG-PET in differentiating infectious from malignant central nervous system lesions in patients with AIDS. J Nucl Med 1992;33:838.
9. Higashi K, Ueda Y, Sakurai A, et al. Correlation of Glut-1 glucose transporter expression with [^{18}F]FDG uptake in non-small cell lung cancer. Eur J Nucl Med 2000;27:1778–85.
10. Chung JH, Coho KJ, Lee SS, et al. Overexpression of Glut 1 in lymphoid follicles correlates with false-positive ^{18}F-FDG PET results in lung cancer staging. J Nucl Med 2004;45:999–1003.
11. Oriuchi N, Higuchi T, Ishikita T, et al. Present role and future prospect of positron emission tomography in clinical oncology. Cancer Sci 2006;97: 1291–7.
12. Chen DL, Dehdashi F. Advances in positron emission tomographic imaging of lung cancer. Pro Am Thorac Soc 2005;2:541–4.
13. Yasukawa T, Yoshikawa K, Aoyagi H, et al. Usefulness of PET with ^{11}C-methionine for the detection of hilar and mediastinal lymph node metastasis in lung cancer. J Nucl Med 2000;41:283–90.
14. Kubota K, Matsuzawa T, Fujiwara T, et al. Differential diagnosis of lung tumor with positron emission tomography: a prospective study. J Nucl Med 1990;31: 1927–33.
15. Tian M, Zhang H, Oriuchi N, Higuchi T, Endo K. Comparison of ^{11}C-choline PET and FDG PET for the differential diagnosis of malignant tumors. Eur J Nucl Med Mol Imaging 2004;31:1064–72.
16. Halter G, Buck AK, Schirrmeister H, et al. [^{18}F]-3-deoxy-3′-fluorothymidine positron emission tomography: alternative or diagnostic adjunct to 2-[^{18}F]-fluoro-2-deoxy-D-glucose positron emission tomography in the workup of suspicious central focal lesion? J Thorac Cardiovasc Surg 2004;127:1093–9.
17. Tomiyoshi K, Amed K, Muhammad S, et al. Synthesis of new fluorine-18 labeled amino acid radiopharmaceutical: L-F-α-methyl tyrosine using separation and purification system. Nucl Med Commun 1997;18:169–75.
18. Inoue T, Tomiyoshi K, Higuchi T, et al. Biodistribution studies on L-[3-^{18}F]-α-methyl tyrosine: a potential tumor-detecting agent. J Nucl Med 1998;39:663–7.
19. Inoue T, Shibasaki T, Oriuchi N, et al. ^{18}F-α-methyl tyrosine PET studies in patients with brain tumors. J Nucl Med 1999;40:399–405.
20. Uchino H, Kanai Y, Kim DK, et al. Transport of amino acid-related compounds mediated by L-type amino acid transporter 1 (LAT1): insights into the mechanisms of substrate recognition. Mol Pharmacol 2002; 61:729–37.
21. Kim DK, Kanai Y, Choi HW, et al. Characterization of the system L amino acid transporter in T24 human bladder carcinoma cells. Biochim Biophys Acta 2002; 1565:112–22.
22. Watanabe H, Inoue T, Shinozaki T, et al. PET imaging of musculoskeletal tumors with fluorine-18 α-methyltyrosine: comparison with fluorine-18 fluorodeoxyglucose PET. Eur J Nucl Med 2000;27:1509–17.
23. Inoue T, Koyama K, Oriuchi N, et al. Detection of malignant tumors: whole-body PET with fluorine-18-α-methyl tyrosine versus FDG-preliminary study. Radiology 2001;220:54–62.
24. Christensen HN. Role of amino acid transport and countertransport in nutrition and metabolism. Physiol Rev 1990;70:43–77.
25. McGivan JD, Pastor-Anglada M. Regulatory and molecular aspects of mammalian amino acid transport. Biochem J 1994;299:321–34.
26. Oxender DL, Christensen HN. Evidence for two types of mediation of neutral amino acid transport in Ehrlich cells. Nature 1963;197:765–7.
27. Kanai Y, Segawa H, Miyamoto K, et al. Expression cloning and characterization of a transporter for large neutral amino acids activated by the heavy chain of 4F2 antigen (CD98). J Biol Chem 1998;273:23629–32.
28. Yanagida O, Kanai Y, Chairoungdua A, et al. Human L-type amino acid transporter 1 (LAT 1): characterization of function and expression in tumor cell lines. Biochim Biophys Acta 2001;1514:291–302.
29. Nawashiro H, Otani N, Shinomiya N, et al. L-type amino acid transporter 1 as a potential molecular target in human astrocytic tumors. Int J Cancer 2006;119: 484–92.
30. Mountain CF, Dresler CM. Regional lymph node classification for lung cancer staging. Chest 1997;111: 1718–23.
31. Oriuchi N, Tomiyoshi K, Inoue T, et al. Independent thallium-201 accumulation and fluorine-18-fluorodeoxyglucose metabolism in glioma. J Nucl Med 1996;37:457–62.
32. Inoue T, Oriuchi N, Kunio M, et al. Accuracy of standardized uptake value (SUV) measured by simultaneous emission and transmission scanning in PET oncology. Nucl Med Commun 1999;20:849–57.
33. Chairoungdua A, Segawa H, Kim JY, et al. Identification of an amino acid transporter associated with the cystinuria-related type II membrane glycoprotein. J Biol Chem 1999;274:28845–8.
34. Matsuo H, Tsukada S, Nakata T, et al. Expression of a system L neutral amino acid transporter at the blood-brain barrier. Neuroreport 2000;11:3507–11.
35. Buck AC, Schirmeister HH, Guhlmann CA, et al. Ki-67 immunostaining in pancreatic cancer and chronic active pancreatitis: does *in vivo* FDG uptake correlate with proliferative activity? J Nucl Med 2001; 42:721–5.
36. Kaira K, Oriuchi N, Otani Y, et al. Diagnostic usefulness of fluorine-18-α-methyltyrosine positron emission tomography in combination with ^{18}F-fluorodeoxyglucose in sarcoidosis patients. Chest 2007;131: 1019–27.
37. Hellwig D, Ukena D, Paulsen F, Bamberg M, Kirsch CM. Meta-analysis of the efficacy of positron emission tomography with F-18-fluorodexyglucose (FDG-PET) in lung tumors as a base for discussion of the German Consensus Conference on PET in Oncology. Pneumologie 2001;55:367–77.
38. Gould MK, Kuschner WG, Rydzak CE, et al. Test performance of positron emission tomography and computed tomography for mediastinal staging in patients with non-small-cell lung cancer. Ann Intern Med 2003;139:879–92.
39. Pauleit D, Floeth F, Tellmann L, et al. Comparison of *O*-(2-^{18}F-fluoroethyl)-L-tyrosine PET and 3-I-iodo-α-methyl-L-tyrosine SPECT in brain tumors. J Nucl Med 2004;45:374–81.
40. Pauleit D, Stoffels G, Schaden W, et al. PET with *O*-(2-^{18}F-fluoroethyl)-L-tyrosine in peripheral tumors: first clinical results. J Nucl Med 2005;46:411–6.
41. Jager PL, Groen HJM, van der Leest A, et al. L-3-^{123}I-iodo-α-methyl-L-tyrosine SPECT in non-small cell lung cancer: preliminary observations. J Nucl Med 2001;42:579–85.
42. Shikano N, Kanai Y, Kawai K, et al. Isoform selectivity of 3-^{123}I-iodo-α-methyl-L-tyrosine membrane transport in human L-type amino acid transporters. J Nucl Med 2003;44:244–6.
43. Nye JA, Schuster DM, Yu W, et al. Biodistribution and radiation dosimetry of the synthetic nonmetabolized amino acid analogue anti-^{18}F-FACBC in humans. J Nucl Med 2007;48:1017–20.
44. Nakanishi K, Matsuo H, Kanai Y, et al. LAT1 expression in normal lung and in atypical adenomatous hyperplasia and adenocarcinoma of the lung. Virchows Arch 2006;448:142–50.
45. Higashi K, Ueda Y, Yagishita M, et al. FDG-PET measurement of the proliferative potential of non-small cell lung cancer. J Nucl Med 2000;41:85–92.
46. Vesselle H, Schmidt RA, Pugsley JM, et al. Lung cancer proliferation correlates with [F-18]fluorodeoxyglucose uptake by positron emission tomography. Clin Cancer Res 2000;6:3837–44.
47. Buck AK, Glatting G, Reske SN. Quantification of ^{18}F-FDG uptake in non-small cell lung cancer: a feasible prognostic marker? J Nucl Med 2004;45: 1274–6.
48. Kobayashi H, Ishii Y, Takayama T. Expression of L-type amino acid transporter 1 (LAT1) in esophageal carcinoma. J Surg Oncol 2005;90:233–8.
49. Parmacek MS, Karpinski BA, Gottesdiener KM, Thompson CB, Leiden JM. Structure, expression and regulation of the murine 4F2 heavy chain. Nucleic Acids Res 1989;17:1915–31.